ACS Photonics

Article

pubs.acs.org/journal/apchd5

Dipolar Resonance Enhancement and Magnetic Resonance in Cross-Coupled Bow-Tie Nanoantenna Array by Plasmonic Cavity

Dihan Hasan,[†,‡,§] Chong Pei Ho,[†,‡,§] Prakash Pitchappa,[†,‡,§] and Chengkuo Lee*[,†,‡,§]

[†]Department of Electrical & Computer Engineering and [‡]Center for Intelligent Sensors and MEMS, National University of Singapore, 4 Engineering Drive 3, 117576 Singapore

[§]NUS Suzhou Research Institute (NUSRI), Suzhou Industrial Park, Suzhou 215123, PR China

Supporting Information

ABSTRACT: We experimentally demonstrate a simple approach for surface current engineering in a cross-coupled bow-tie nanoantenna by inserting a plasmonic cavity that simultaneously offers (i) improved Fano-like dipolar resonance contrast, (ii) electrically induced magnetic resonance, and (iii) enhanced sensitivity. By introducing a small geometric perturbation, we propose two physical parameters, offset (*f*) and split gap (*s*), for strong modulation of resonance location and intensity. We report at least 3.75-fold better dipolar resonance compared with the conventional design and demonstrate a unique mechanism for exciting magnetic plasmonic resonance. Finally, we obtain a large wavelength shift of 777.5 and 904 nm per refractive index unit (RIU) with a thin PMMA coating (110 nm) for the dipolar resonance and magnetic resonance, respectively. Numerical study indicates the potential of the proposed bow-tie nanoantenna array structure with a self-similar plasmonic cavity (SSP BNA) for sensitive recording of binding events of molecules such as DNA by reestablishing conduction current and providing "on" and "off" states. The high-density plasmonic antenna array structure will be promising for engineering applications in optical magnetism, magnetoplasmonics, optical trapping, and massively parallel ultrasensitive differential detection of molecular fingerprints.

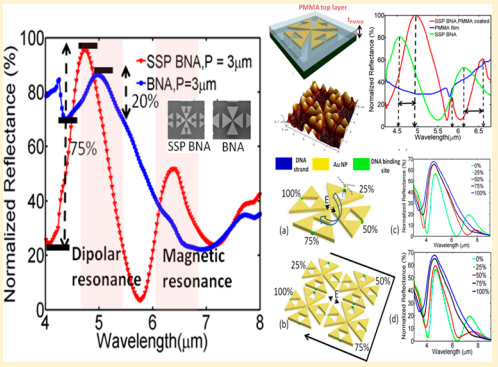

KEYWORDS: *bow-tie nanoantenna, dipolar resonance, Fano effect, magnetic resonance, plasmonic cavity, subwavelength hotspots*

In the last few years, the field of plasmonics received extensive attention of researchers because of plasmon's formidable ability to couple free-space electromagnetic excitation into nanoscale volume and enhance near-field optical intensity. Such an exotic advantage of metal optics paves the way for engineering light−matter interaction more feasibly. With the recent advancement of nanotechnology, plasmonics has become a burgeoning research topic in energy-harvesting, telecom, and sensing industries.[1−5] Among various categories of nanostructures reported so far to manipulate localized surface plasmon resonance (LSPR), bow-tie nanoantennae hold a unique position because of their giant electric field enhancement at the sharp metal tips and nanofocusing characteristics. Hence, bow-tie nanostructures have been used for high-performance plasmonic applications such as nanolithography,[6] ultralow-power optical trapping,[7] single-molecule fluorescence detection,[8] extreme UV generation,[9] and plasmonic photography film for high-density storage.[10] Variations of bow-tie nanostructure have also been found to be of significant engineering merit to enhance nonlinear optical effects lately.[11−13] However, no significant work has been reported to refine bow tie shape in order to mediate large damping of plasmons in noble metals at midinfrared (IR) wavelengths.

In contrast, there has been a tremendous research interest as well to explore novel approach of controlling properties of plasmons. Among these approaches, magneto plasmonics is an emerging niche of research in order to achieve magneto optic modulation of plasmons and plasmon-mediated magnetic recording devices.[14−17] Recently, bifunctional plasmonic−magnetic devices have been demonstrated for magnetic-field-controlled optical modulation and surface-enhanced Raman spectroscopy sensors.[18,19] However, most of such concepts rely upon the integration of ferromagnetic and plasmonic materials, making the fabrication process much challenging. However, artificial optical magnetism in nonmagnetic materials has not been feasible because of their low magnetic polarizability until Pendry et al. proposed the split ring meta atom in 1999.[20] Since then, split ring resonators (SRR) have been demonstrated over different ranges of spectra from visible to terahertz.[21,22] Enhanced functionalities of this fundamental building block, i.e., SRR, by using CMOS-compatible microelectromechanical (MEM) tuning mechanisms have also been demonstrated recently.[23−25]

Previously, several configurations of bow-tie nanostructures such as diabolo and capped nanoantenna have been theoretically investigated for magnetic field enhancement.[26−28] However, the designs either have poor electric field

Received: February 27, 2015
Published: June 11, 2015

DOI: 10.1021/acsphotonics.5b00088
ACS Photonics 2015, 2, 890−898

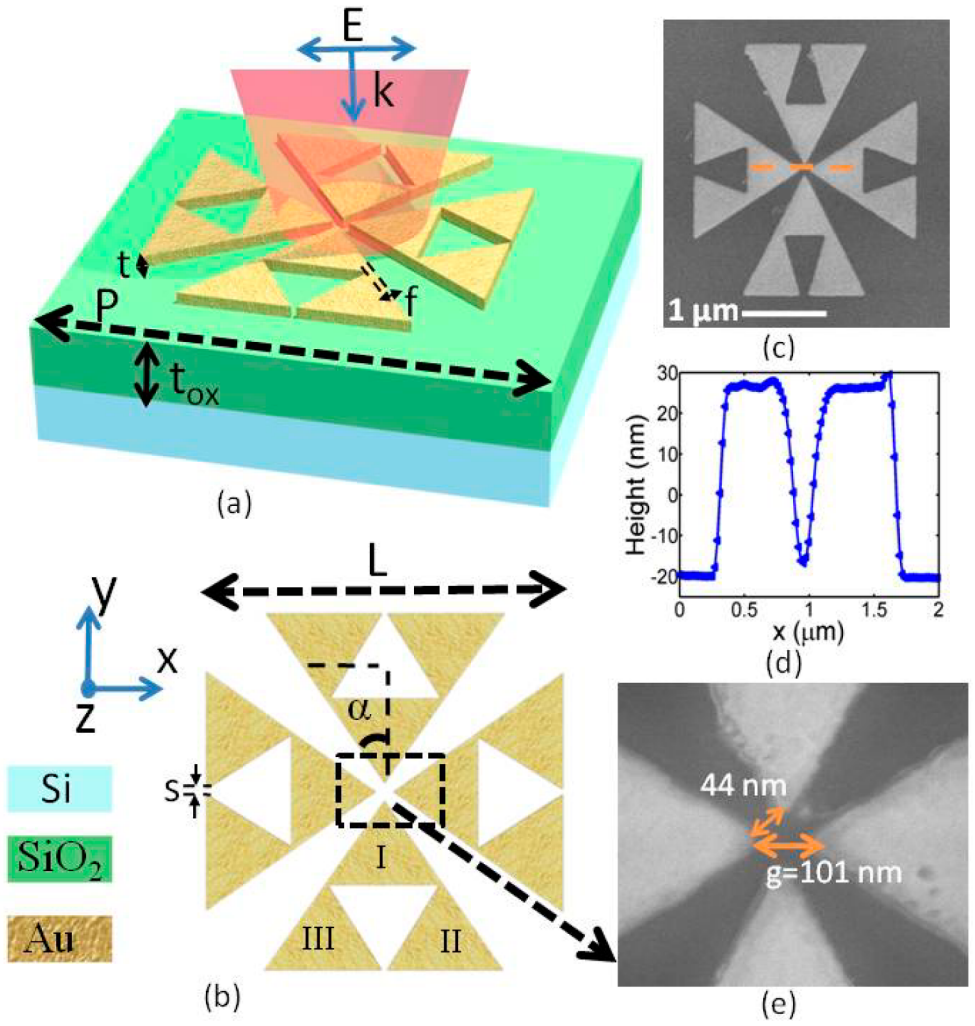

Figure 1. (a) 3D schematic drawing of the proposed bow-tie antenna structure (BNA) with a self-similar plasmonic cavity (SSP) denoted as SSP BNA. (b) Top view of the unit cell. (c) SEM image of the fabricated structure. (d) Height profile of AFM scan line along the coupling gap. (e) Zoom-in view of SEM image of the fabricated bow tie tips.

enhancement or rely on complex fabrication process. In this work, we experimentally report a multifunctional plasmonic–magnetic bow-tie nanostructure that demonstrates simultaneous enhancement of electric and magnetic fields and can be realized by a simpler fabrication method. The proposed polarization-independent structure is a proof-of-concept demonstration of surface current engineering in bow-tie antenna by sharp metal corners that offers both magnetic resonance and significantly improved dipolar characteristics compared to its conventional counterpart. Besides, we demonstrate that the proposed cross-coupled high-density plasmonic array of bow-tie structures can potentially have a large RIU shift around the two specific bands of interest which are spectrally and spatially distinct from each other under single polarization (TE or TM). Such a dual-band scheme is significantly unique to the previous approach that is based on electrical and cavity resonance[29−31] in a sense that the near-field enhancement by the deep subwavelength hotspots of the 2D metal patterns are directly accessible to the surrounding substance. Our study also anticipates that the design can potentially stand out as a platform for DNA programmable devices by leveraging the increased number of hotspots and strong cross-coupling obtained at a proximity of tens of nanometers.

DESIGN

Figure 1 shows the detailed configuration of the unit cell bow-tie nanoantenna (BNA) with a self-similar plasmonic cavity (SSP) and the fabricated device. The cavity is symmetrically inserted into each of the four bow-nanoantenna triangles by joining the mid points of their sides. Furthermore, by introducing small geometric perturbation, two design parameters, split gap (s) and offset (f), are deployed to modulate the surface current density. Thus, we subdivide a single host isosceles triangle into three nearly identical smaller triangles (I, II and III). In this work, the following parameters are fixed: Au thickness t = 35 nm, coupling gap g = 100 nm, antenna length L = 2.55 μm, and pitch P = 3 μm, whereas we achieve a minimum cross-coupling gap of 44 nm between the horizontal and vertical triangles at apex angle α = 30°.

We also investigate a conventional BNA without SSP with similar parameters in order to make a comparison. Both structures are fabricated on Si wafer coated with a t_{ox} = 1 μm thick SiO_2 top layer using high-resolution ELS-7000 electron-beam lithography (Supporting Information). A 3D FDTD solver has been deployed to obtain the near-field characteristics of the structures (Supporting Information). Figure 2a,b shows that the experimental results are qualitatively consistent with

DOI: 10.1021/acsphotonics.5b00088
ACS Photonics 2015, 2, 890−898

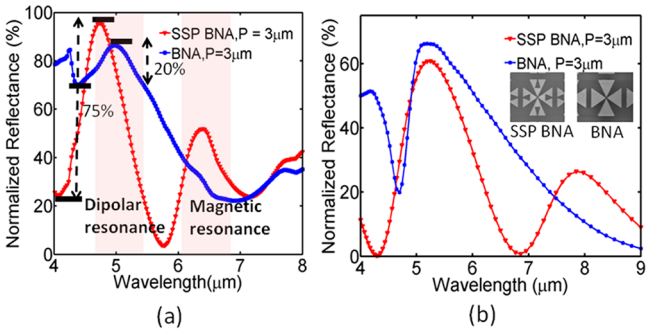

Figure 2. Measured reflection spectra: (a) experiment (b) simulation. The inset shows the fabricated samples of BNA and SSP BNA. The values of *s*, *f*, *α*, *g*, and *P* are fixed at 100 nm, 100 nm, 30°, 100 nm, and 3 *μ*m, respectively.

the simulated results, although a strong blueshift (∼0.25−1 *μ*m) is observed in the far-field resonance spectrum compared to the near-field spectrum. Such a blueshift is a well-known phenomenon in strongly scattering metal patterns in the presence of large plasmonic damping.[32,33] Additional shift can be attributed to the structural imperfections and dispersion of oxide layer over the large bandwidth. Slight deviation of resonance spectrum shape in experimental data can be further ascribed to specular reflectance setup of the FTIR. Nevertheless, the SSP BNA structure not only exhibits the additional magnetic resonance but also enhances the dipolar resonance contrast significantly in the far field measurement. We plot the field profiles and the surface current distribution at the near-field peak locations in Figure 3. By comparing the data in Figure 3e with the data in Figure 3b, the peak magnetic field intensity $|H_0|^2/|H_{in}|^2$ is improved sixfold at dipolar resonance because of the presence of the plasmonic cavity. Such enhancement can be directly correlated with the surface current distributions as shown in Figure 3c,f. The peak electric field intensities $|E_0|^2/|E_{in}|^2$ in Figure 3a,d at dipolar resonance are comparable to each other. However, the field distribution in SSP BNA is spatially different because of the presence of the split gap at the bottom of the each triangular arm.

Modified dipolar characteristics of nanorod antenna configured into a V shape has been previously reported by Capasso et. al.[34] Similarly, the origin of the dipolar resonance enhancement in the SSP BNA structure can be traced back to two distinct features of the geometry. First, the surface area of each triangle of the SSP BNA structure can be treated as a combination of three nearly identical subwavelength radiators (radiators I−III) coherently coupled to each other as shown in Figure 1a. Because of their self-similar arrangement, they can augment the far-field reflection when they resonate con-

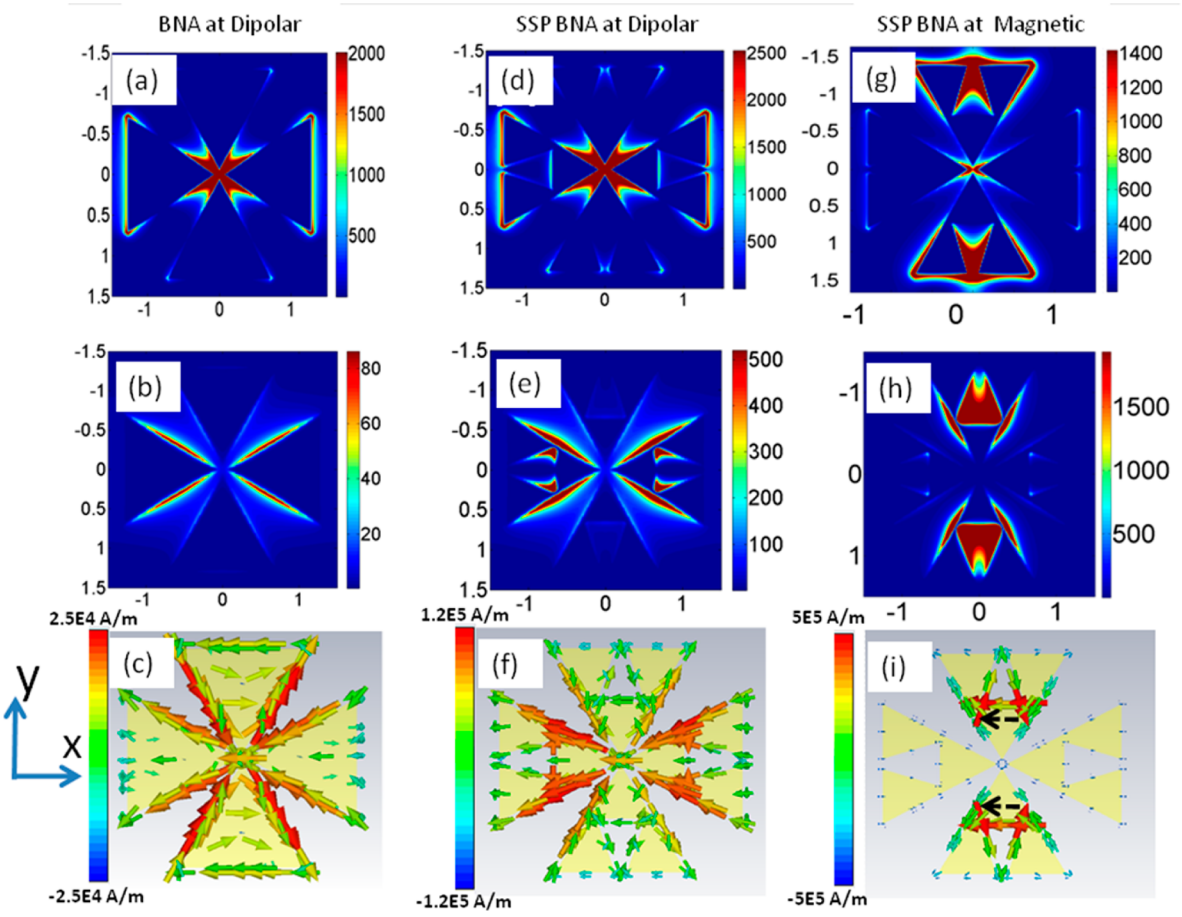

Figure 3. (a) Electric field intensity, (b) magnetic field intensity, and (c) surface current distribution along the midplane of the BNA at 5 *μ*m (dipolar resonance). (d) Electric field intensity, (e) magnetic field intensity, and (f) surface current distribution along the midplane of the SSP BNA at 5 *μ*m (dipolar resonance). (g) Electric field intensity, (h) magnetic field intensity, and (i) surface current distribution along the midplane of the SSP BNA at 7.5 *μ*m (magnetic resonance). The values of *s*, *f*, *α*, *g*, and *P* are fixed at 100 nm, 100 nm, 30°, 100 nm, and 3 *μ*m, respectively. The black dashed arrows marked in i indicate the dominant component of circular current. The incident light is polarized along *x* axis.

DOI: 10.1021/acsphotonics.5b00088
ACS Photonics 2015, 2, 890−898

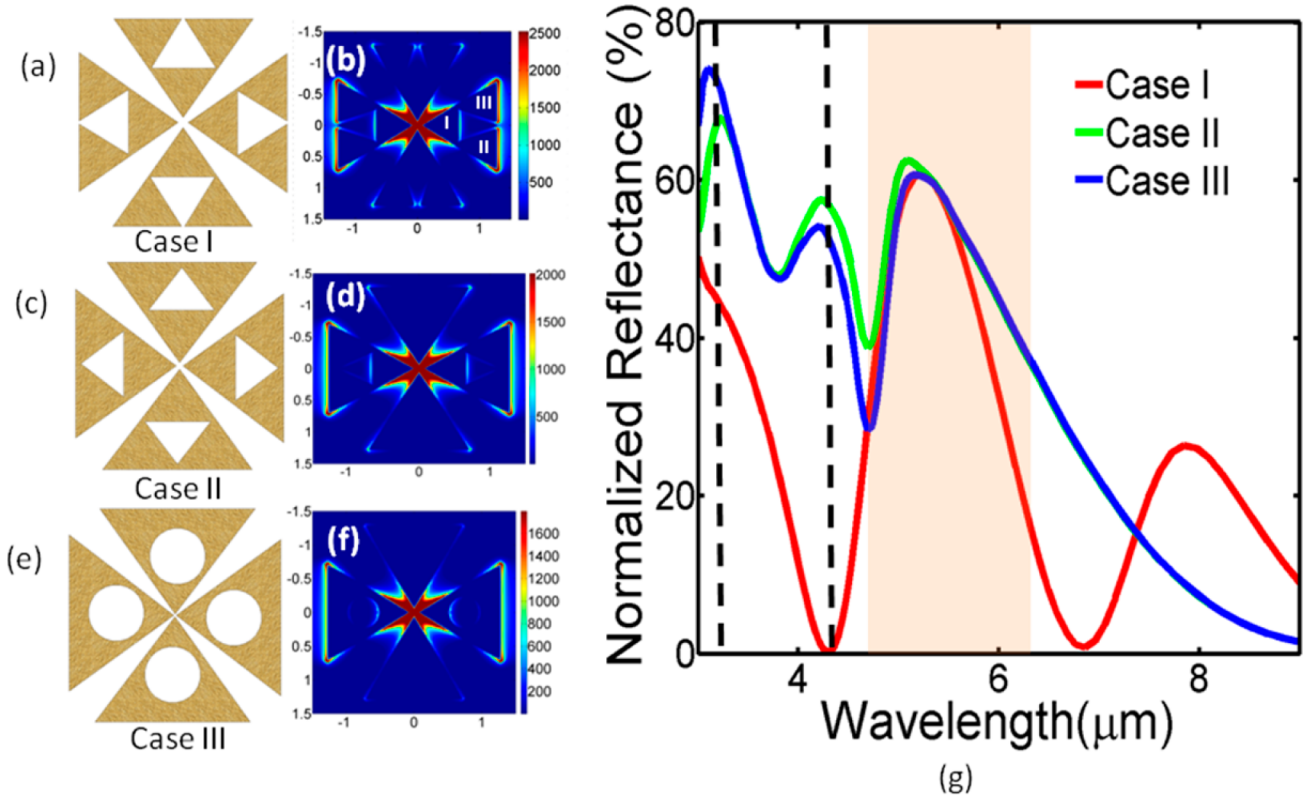

Figure 4. (a) Case I (SSP BNA) layout, (b) E-field in case I at 5 μm, (c) Case II layout, (d) E-field in case II at 5 μm, (e) Case III layout, (f) E-field in case III at 5 μm, and (g) simulated spectra of three cases. The dashed lines indicate the quadruplerlike resonances from the vertical pair of triangles. In all cases, the minimum offset (f) between the void and the edge of large triangle is kept constant at 100 nm.

structively at the same wavelength. Second, the unique structure of SSP BNA unit cell boosts the surface current density because of the presence of the sharp corners and the narrow conduction path. For x-polarized light, the bottom radiators II and III are forced to strengthen the current at their meeting points with radiator I because of the presence of the split gap. Thus, the split gap pushes more electrons toward the narrow junctions and strongly influences the E-field along the bottom edge of the dipolar triangles. The current density $J(x, y)$ in SSP BNA still follows a dipolarlike distribution while experiencing an amplification at the narrow junction as shown in Figure 3f. Because of the triangular shapes of the radiators, we find that both $J(x)$ and $J(y)$ are amplified through this process. In fact, the peak current density (A/m) in SSP BNA structure at dipolar resonance (Figure 3f) is 4.8 times larger than that in BNA structure (Figure 3c). The overall enhancement of $J(x, y)$ in SSP BNA can contribute to the increase of the net dipole moment (p) of the structure according to $p = ((1)/(-j\omega))\int_V J(x, y, z)\, dV$, where V is the total volume of integration.[35] Such intuitive engineering of moment is practical for bow-tie nanostructure because a large portion of the dipolar current flows along the edges. More clearly speaking, resonance contrast can increase because of reduced reflection by reduced metal surface area at off-resonance because we include void or air gap in the antenna arms. However, the proposed mechanism is a systematic approach to increase dipolar resonance contrast of bow-tie nanostructure by surface current engineering which can be verified by considering two other cases, i.e., case II (Figure 4b): triangular voids without any split gap and case III (Figure 4c): circular voids with open area equal to that of case I (Figure 4a). Figure 4g shows that the SSP BNA (case I) clearly outperforms case II and case III in terms of contrast and quality factor (Q) of dipolar resonance. Such result justifies the merit of surface current engineering in SSP BNA with the help of narrow corners and a split gap. It also shows that the split gap can efficiently suppress the quadruplerlike resonances at shorter wavelengths in a polarization independent configuration. In this work, with the help of the optimized approach, we experimentally observe at least 75% resonance contrast in a highly dense SSP BNA as opposed to 20% in conventional BNA under the Fano condition obtained by strong diffractive coupling at $P = 3$ μm (Supporting Information).

Figure 3g,h,i shows the E-field, H-field, and the surface current distribution, respectively, in SSP BNA when the magnetic plasmonic resonance occurs. The magnetic field distribution in the proposed geometry is largely in contrast with that of a conventional split-ring layout because it has multiple magnetic hotspots (Figure 3h) arising from the amplified current density in the narrow conduction path and a totally different displacement field distribution. In contrast, we observe dual electric field hotspots (Figure 3g) of deep subwavelength volume ($V/\lambda^3 \approx 10^{-6}$) at the split gap of the resonator by the circulating current indicated in Figure 3i and at the tip of the bow-tie triangle because of the cross-coupled configuration. Thus, the proposed split gap in the design has two important contributions: enhancement of dipolar resonance and electrical excitation of magnetic resonance.

STUDY OF PARAMETERS

The modulation of the optical resonance spectra as a function of offset (f) and split gap (s) is shown in Figure 5. The whole

DOI: 10.1021/acsphotonics.5b00088
ACS Photonics 2015, 2, 890−898

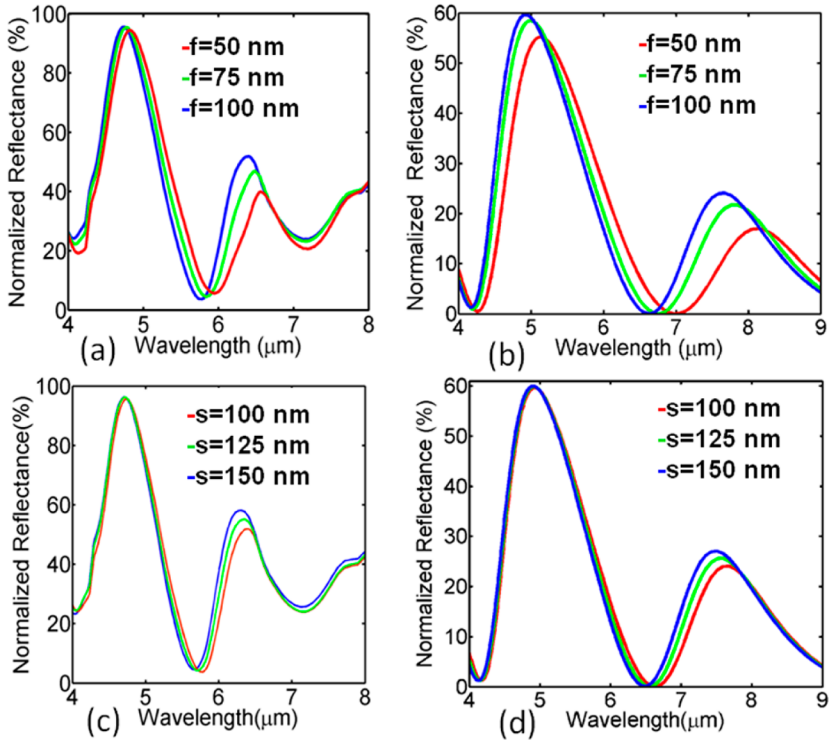

Figure 5. (a) Experimental data and (b) simulation data of effect of offset (f) on array reflectance. (c) Experimental data and (d) simulation data of effect of split gap (s) on array reflectance.

spectrum shows redshift as f is decreased because a decrease of f at a fixed s will increase the surface current density to some extent. For dipolar resonance, the coherent interaction among the three constituent radiators of each triangle gets stronger when the current density becomes high. Stronger interaction among coherent radiators is finally interpreted as a redshift of dipolar resonance as shown in Figure 5a. This is also in agreement with the simulation results in Figure 5b. As f is increased, slight improvement of dipolar resonance intensity in simulation can be attributed to two factors: (i) net dipole moment as a function of metal surface area and (ii) increased back ground reflection. Such resonance enhancement can also be inferred from experimental results. In contrast, the influence of varying s on dipolar resonance is found to be less significant in both experiment and simulation as shown in Figure 5c,d. This is because the split gap cannot impact the strength of dipolar surface current flowing along the edges of the resonant triangles. However, the modulation characteristics of magnetic resonance as a function of f are in deep contrast with that of dipolar resonance. It can be seen that experimental resonance wavelength linearly shifts by 200 nm starting from 6.57 to 6.37 μm as f is increased from 50 to 100 nm. Such blueshift can be explained by plasmonic hybridization model. Figure 3j shows that the dominant component of the circulating current marked with dashed arrow is flowing along the horizontal edge (parallel to the x axis) of the triangular resonator. This implies the accumulation of positive and negative charges at the opposite ends of this edge. As f is increased, the gap between them is decreased; hence, the restoring force is increased. Although the charge density decreases as f is increased, the effect of this gap is more dominant because of inverse square dependence of Coulombic interaction. Because higher restoring force means higher oscillation frequency, the overall energy state of the plasmonic structure shifts to shorter wavelengths.[36] The observed wavelength shift can also be explained partially by circuit theory. As f is decreased, we can assume that the effective width of the junction at the corners is decreased, and it will eventually increase the effective inductance (L) for a given condition. Subsequently, the magnetic resonance wavelength $\lambda \propto (LC)^{1/2}$ will show a redshift.[37] This is a unique approach for inductive tuning of magnetic resonance by utilizing localized current density, whereas it is not possible in conventional split-ring structure. The increase of resonance intensity as f is increased can be related to the improvement of total magnetic moment, $m = (^1/_2)\int Vr' \times J(r')\, dV$, which depends on the area of metal junctions.[35,38] On the contrary, the effect of varying s on resonance location and intensity is rather straightforward. It can be observed in Figure 5c,d that the magnetic resonance experiences blueshift as s is increased following the relationship $C \propto 1/s$ between the capacitance and split gap.[38] The resonance enhancement is attributed to the increased magnetic moment as the gap is increased for capacitive tuning. Between the two parameters, f and s, we find in our experiment that the role of f is more crucial for tuning the resonance intensity and location (Supporting Information). This is because f can directly alter the dominant surface current at magnetic resonance as shown in Figure 3j and thus can modulate the electrical response from the dominant edge of the cavity and the magnetic response from the circular current. On the contrary, s can only influence the magnetic response in a capacitive way.

Apex angle is another unique parameter of bow-tie geometry for coarse tuning of resonance over a large bandwidth. Here, we vary the angle from 15 to 30° in our experiment. Figure 6 shows E- and H-field distribution at dipolar and magnetic resonance for these two angles, respectively.

It is observed in Figure 7a that both the resonances blue-shift and decrease in intensity as the angle is reduced. The shift of

DOI: 10.1021/acsphotonics.5b00088
ACS Photonics 2015, 2, 890−898

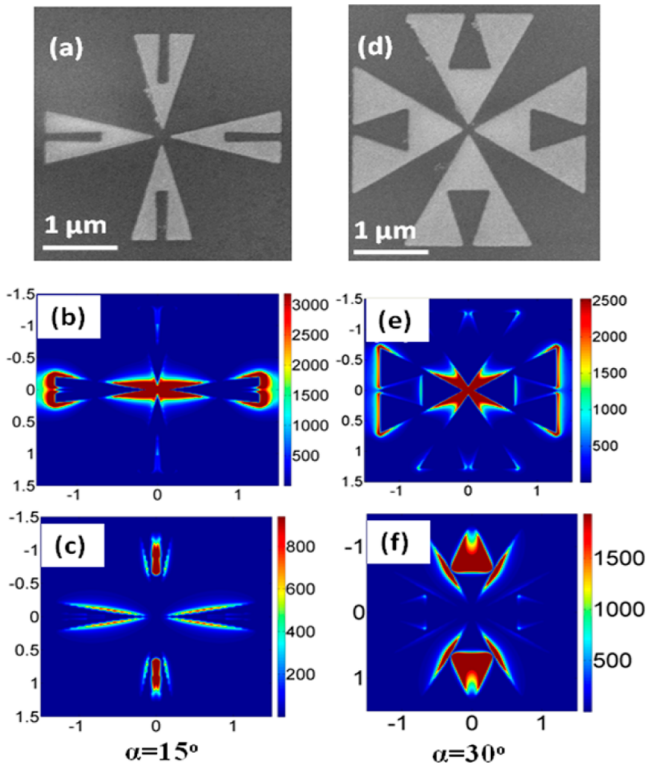

Figure 6. (a) SEM, (b) E-field distribution at dipolar resonance (4.7 μm), and (c) H-field distribution at magnetic resonance (5.7 μm) for SSP BNA with α = 15°. (d) SEM, (e) E-field distribution at dipolar resonance (4.9 μm), and (f) H-field distribution at magnetic resonance (7.15 μm) for SSP BNA with α = 30°.

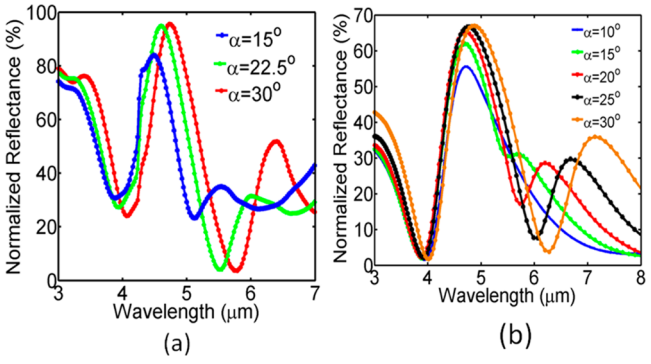

Figure 7. Effect of apex angle: (a) experiment and (b) simulation.

dipolar resonance is mainly attributed to the reduction of effective length of the side edges. The drop in resonance intensity and contrast occurs as the cross coupling shown in Figure 6b,e between the horizontal and the vertical pair is weakened. The magnetic resonance shift is due to the decrease of effective inductance with the decrease of the area of current loop. The overall magnetic moment is also likely to be affected as the resonance contrast keeps decreasing with the decrease of apex angle. The simulation results in Figure 7b obtained in the absence of any substrate-induced resonance are also in good agreement with the experimental results. The weakening of magnetic response can be correlated with the difference of magnetic field intensity in Figure 6c,f as well. The simulation result at α = 10° in Figure 7b suggests that overlapping of dipolar mode and magnetic mode is achievable in the proposed nanoarchitecture by careful design.

To further investigate the role of cross coupling, we consider another unique structure as shown in the inset of Figure 8a,

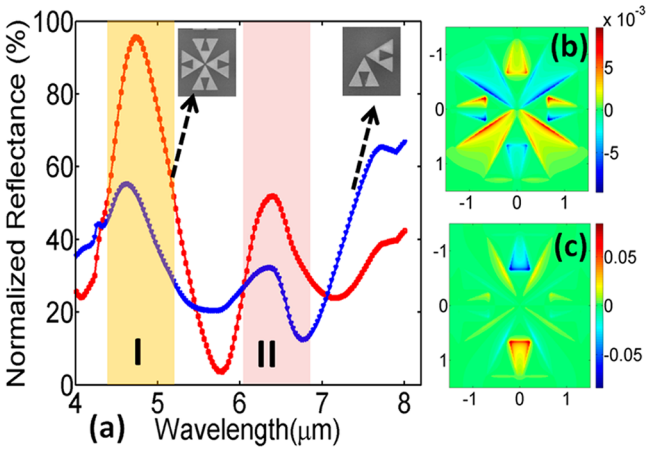

Figure 8. (a) Effect of cross coupling on resonance. Phase map of real (Hz) (b) dipolar resonance, I, and (c) magnetic resonance, II.

removing the opposite triangles that were resonantly matched before and without breaking the polarization independence. It is quite clear that the original cross-coupled structure outperforms the modified one. The dipolar and the magnetic resonance intensity drops by 40 and 23%, respectively, as we migrate from the original structure to the modified one. In the modified structure, the dipolar−dipolar and charge−charge interaction are missing and dipolar−-charge interaction is weakened alongside the weakening of near field array effect.[39] Because of these combined effects, we see noticeable degradation of dipolar resonance intensity. However, the weakening of magnetic resonance is primarily attributed to the weakening of near-field coupling effect. The phase maps for dominant component of magnetic field (in hertz) in Figure 8b,c illustrate the contrast of in-phase interaction between the transverse and longitudinal triangle pairs at different resonances. Such nearly coherent interaction can pump more charges into the active components and boost up the intensity of resonance.

APPLICATIONS

We demonstrate the potential of the device for nanoantenna-enhanced ultrasensitive spectroscopy. Figure 9a shows the schematic for the experiment. Figure 9b shows the AFM image of the spin-coated sample. The normalized reflectance profile in Figure 9c shows that the C═O absorption peak of PMMA at 5.8 μm can be strongly captured by the current design.[40] The experimentally observed wavelength shift for such thin layer coating (110 nm) is found to be 381 and 443 nm for dipolar and magnetic resonance, respectively. This gives an RIU shift of 777.5 and 904 nm for dipolar and magnetic resonance, respectively, at n_{PMMA} = 1.49. The simulated values obtained by changing the bulk background index by 10% are 1880 and 3010 nm, respectively, whereas the simulated value obtained for BNA is 1000 nm. The experimental shift is comparable to or even better than the recent result (1010 nm) reported in ref 3, in the sense that the interaction volume in our case is much smaller than in a bulk solution. Such dual-band large shift is attributed to the presence of plasmonic cavity, strong cross coupling, and near-field interaction. Magnetic resonance experiences a larger shift because it has higher spatial coverage

DOI: 10.1021/acsphotonics.5b00088
ACS Photonics 2015, 2, 890−898

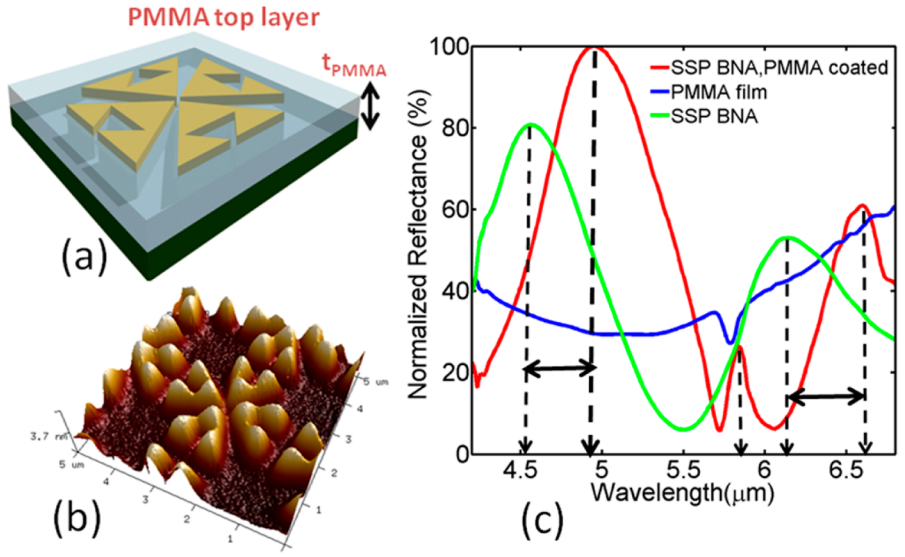

Figure 9. (a) Schematic of the SSP BNA enhanced spectroscopy. (b) AFM image of SSP BNA coated with 110 nm PMMA. (c) Normalized spectra under different conditions. The values of *s*, *f*, *P*, and *g* are fixed at 200 nm, 100 nm, 3 μm, and 200 nm, respectively.

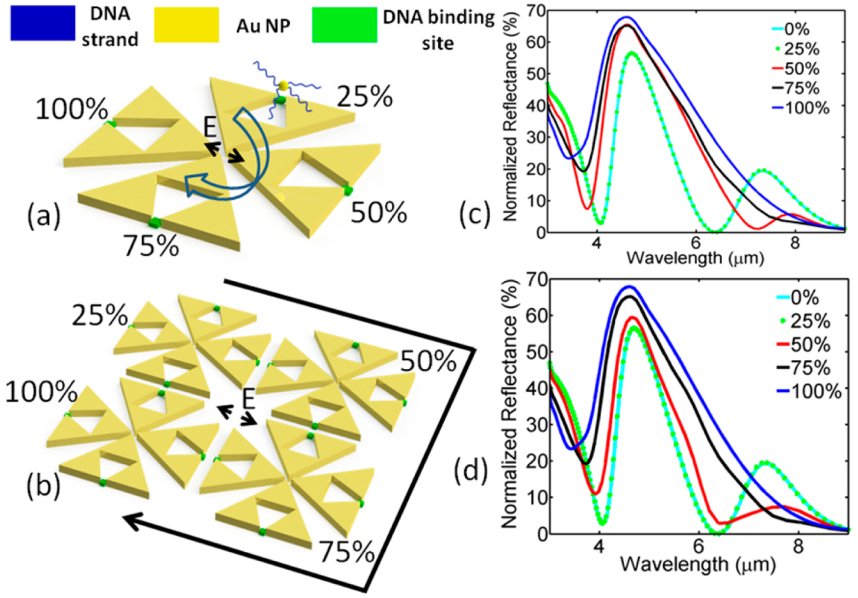

Figure 10. (a) Conceptual schematic of DNA tuning of the proposed SSP BNA nanostructure. (b) DNA binding spots in a 2 × 2 array. Simulated effects of different percentages of DNA binding events on the reflection spectrum within (c) a unit cell and (d) within an area of 36 μm^2 covering a 2 × 2 array. The diameter of the nanoparticle (NP) is 100 nm, matched with the width of split gap.

than the dipolar resonance. We also observe nearly 100% reflection by the dipolar resonance in Figure 9c when the thin metal patterns (~40 nm) are coated with a PMMA layer.

Besides, the strong effect of split gap on the overall resonance spectrum can be efficiently exploited for precise molecular detection and reconfiguration. In Figure 10a, a conceptual schematic of DNA-mediated assembly of Au nanoparticle into the structure is illustrated.[41] In addition to the commonly perceived tip-to-tip central gap in bow-tie nanostructure, the proposed design offers four extra hotspots for enhanced reconfiguration of plasmonic device using DNA technology. The binding site can be realized by an additional EBL step within an accuracy of few nanometers. As shown in Figure 10c, with the help of its spatially distinctive dual resonances the unit cell can successfully register binding event percentage as low as 50% under *x*-polarization when two hotspots, one from the vertical pair and one from the horizontal pair, are functionalized and conduction current is partially reestablished. The detailed definition of binding percentage is clearly illustrated in Figure 10a. A complete "on−off" state can be achieved for magnetic resonance when both of the vertical hotspots are functionalized (75%). The role of strong cross coupling on dipolar resonance is also quite evident at this point. Finally, a 15% diminution of dipolar resonance contrast along with a noticeable reduction of *Q* (associated with a 500 nm blue-shift of resonance dip) is observed at 100% binding success. Because of the Fano condition and strong near-field coupling maintained at $P = 3$ μm, the design can be also useful for reliable detection under random scenarios. We consider the test configuration shown in Figure 10b. In an area 6 μm × 6 μm, we gradually increase the number of fully functionalized unit cells (25, 50, 75, and 100%). As indicated by Figure 10d, complete switching of magnetic

DOI: 10.1021/acsphotonics.5b00088
ACS Photonics 2015, 2, 890−898

resonance is possible at 75% success rate according to this model along with a pronounced change in dipolar peak. With the help of our particular experimental findings on Fano effect and strong cross coupling and theoretical binding model, it can be concluded that the proposed design is highly suitable for robust detection of random events.

CONCLUSIONS

We experimentally demonstrate a simple yet systematic approach that is based on surface current engineering to compensate for damping of plasmons at mid-IR range and enhance the bow tie dipolar resonance contrast under Fano condition. Artificial magnetism obtained by this approach will pave the way for bow-tie nanostructures to be treated as a building block of negative index metamaterial for sharp-tip-enhanced applications.[42] We conduct an in-depth experiment and identify the critical role of split gap, offset, vertex angle, and cross coupling for the optimization of the device characteristics. We experimentally report that the proposed configuration can obtain a very large sensitivity because of its strongly interacting nature and may offer a dual-band differential detection mechanism of bulk and surface contribution.[43] Moreover, the presence of carefully chosen plasmonic voids can enable SSP BNA for applications such as single-molecule detection and DNA programmability with improved signal-to-noise ratio and higher reliability.[44−46] This simple approach can be systematically scaled up to increase the number of hotspots to as high as 17 in 1 unit cell within the limit of nanofabrication and extended further for designing polarization-independent ultracompact, multiplexed, multispectral magnetic sensors, thermal cameras, and electromagnetic energy harvesters over a broad range of infrared spectrum.

ASSOCIATED CONTENT

Supporting Information

Discussion on fabrication, simulation, measurement and additional results. The Supporting Information is available free of charge on the ACS Publications website at DOI: 10.1021/acsphotonics.5b00088.

AUTHOR INFORMATION

Corresponding Author

*E-mail: elelc@nus.edu.sg.

Notes

The authors declare no competing financial interest.

ACKNOWLEDGMENTS

The authors acknowledge the financial support from the research grant of, MOE/NUS, ARF-Tier 2 (MOE2012-T2-2-154; NUS WBS: R-263-000-A59-112) "Monolithic integrated Si/AlN nanophotonics platform for optical NEMS and OEICs" at the National University of Singapore, and the partial support by National Natural Science Foundation of China under grant no. 61474078 at NUS (Suzhou) Research Institute, Suzhou, China.

REFERENCES

(1) Karker, N.; Dharmalingam, G.; Carpenter, M. A. Thermal Energy Harvesting Plasmonic Based Chemical Sensors. *ACS Nano* **2014**, *8*, 10953−10962.

(2) Dregely, D.; Lindfors, K.; Lippitz, M.; Engheta, N.; Totzeck, M.; Giessen, H. Imaging and steering an optical wireless nanoantenna link. *Nat. Commun.* **2014**, *5*, 4354.

(3) Shen, Y.; Zhou, J.; Liu, T.; Tao, Y.; Jiang, R.; Liu, M.; Xiao, G.; Zhu, J.; Zhou, Z.; Wang, X.; Jin, C.; Wang, J. Plasmonic gold mushroom arrays with refractive index sensing figures of merit approaching the theoretical limit. *Nat. Commun.* **2013**, *4*, 2381.

(4) Xu, X.; Hasan, D.; Wang, L.; Chakravarty, S. Guided-mode-resonance-coupled plasmonic-active SiO_2 nanotubes for surface enhanced Raman spectroscopy. *Appl. Phys. Lett.* **2012**, *100*, 191114.

(5) Ren, F.; Campbell, J.; Hasan, D.; Wang, X.; Rorrer, G. L.; Wang, A. X. Bio-Inspired Plasmonic Sensors by Diatom Frustules. In *Proceedings of CLEO: Science and Innovations*, San Jose, California, June 9−14, 2013; OSA Publishing: Washington, D.C., 2013; CTh3I.4.

(6) Pan, L.; Park, Y.; Xiong, Y.; Ulin-avila, E.; Wang, Y.; Zeng, L.; Xiong, S.; Rho, J.; Sun, C.; Bogy, D. B.; Zhang, X. Maskless Plasmonic Lithography at 22 nm Resolution. *Sci. Rep.* **2011**, *1*, 1−6.

(7) Roxworthy, B. J.; Ko, K. D.; Kumar, A.; Fung, K. H.; Chow, E. K. C.; Liu, G. L.; Fang, N. X.; Toussaint, K. C. Application of plasmonic bowtie nanoantenna arrays for optical trapping, stacking, and sorting. *Nano Lett.* **2012**, *12*, 796−801.

(8) Kinkhabwala, A.; Yu, Z.; Fan, S.; Avlasevich, Y.; Müllen, K.; Moerner, W. E. Large single-molecule fluorescence enhancements produced by a bowtie nanoantenna. *Nat. Photonics* **2009**, *3*, 654−657.

(9) Sivis, M.; Duwe, M.; Abel, B.; Ropers, C. Extreme-ultraviolet light generation in plasmonic nanostructures. *Nat. Phys.* **2013**, *9*, 304−309.

(10) Roxworthy, B. J.; Bhuiya, A. M.; Inavalli, V. V.; Chen, H.; Toussaint, K. C. Multifunctional Plasmonic Film for Recording Near-Field Optical Intensity. *Nano Lett.* **2014**, *14*, 4687−4693.

(11) Aouani, H.; Navarro-Cia, M.; Rahmani, M.; Sidiropoulos, T. P. H.; Hong, M.; Oulton, R. F.; Maier, S. A. Multiresonant Broadband Optical Antennas As Efficient Tunable Nanosources of Second Harmonic Light. *Nano Lett.* **2012**, *12*, 4997−5002.

(12) Navarro-Cia, M.; Maier, S. A. Broad-Band Near-Infrared Plasmonic Nanoantennas for Higher Harmonic Generation. *ACS Nano* **2012**, *6*, 3537−3544.

(13) Hess, O.; Pendry, J. B.; Maier, S. A.; Oulton, R. F.; Hamm, J. M.; Tsakmakidis, K. L. Active nanoplasmonic metamaterials. *Nat. Mater.* **2012**, *11*, 573−584.

(14) Armelles, G.; Cebollada, A.; García-Martín, A.; Ujué González, M. Magnetoplasmonics: Combining Magnetic and Plasmonic Functionalities. *Adv. Opt. Mater.* **2013**, *1*, 10−35.

(15) Chen, J.; Albella, P.; Pirzadeh, Z.; Huth, F.; Bonetti, S.; Bonanni, V.; Vavassori, P.; Dmitriev, A.; Aizpurua, J.; Hillenbrand, R. Plasmonic Nickel Nanoantennas. *Small* **2011**, *7*, 2341−2347.

(16) Bonanni, V.; Bonetti, S.; Pakizeh, T.; Pirzadeh, Z.; Chen, J.; Nogués, J.; Vavassori, P.; Hillenbrand, R.; Åkerman, J.; Dmitriev, A. Designer Magnetoplasmonics with Nickel Nanoferromagnets. *Nano Lett.* **2011**, *11*, 5333−5338.

(17) Belotelov, V. I.; Kreilkamp, L. E.; Akimov, I. A.; Kalish, A. N.; Bykov, D. A.; Kasture, S.; Yallapragada, V. J.; Gopal, A. V.; Grishin, A. M.; Khartsev, S. I.; Nur-E-Alam, M.; Vasiliev, M.; Doskolovich, L. L.; Yakovlev, D. R.; Alameh, K.; Zvezdin, A. K.; Bayer, M. Plasmon-mediated magneto-optical transparency. *Nat. Commun.* **2013**, *4*, 2128.

(18) Temnov, V. V. Ultrafast acousto-magneto-plasmonics. *Nat. Photonics* **2012**, *6*, 728−736.

(19) Xu, X.; Li, H.; Hasan, D.; Ruoff, R. S.; Wang, A. X.; Fan, D. L. Near-Field Enhanced Plasmonic-Magnetic Bifunctional Nanotubes for Single Cell Bioanalysis. *Adv. Funct. Mater.* **2013**, *23*, 4332−4338.

(20) Pendry, J. B.; Holden, A. J.; Robbins, D. J.; Stewart, W. J. Magnetism from conductors and enhanced nonlinear phenomena. *IEEE Trans. Microwave Theory Tech.* **1999**, *47*, 2075−2084.

(21) Tobing, L. Y.; Tjahjana, L.; Zhang, D. H.; Zhang, Q.; Xiong, Q. Sub-100-nm Sized Silver Split Ring Resonator Metamaterials with Fundamental Magnetic Resonance in the Middle Visible Spectrum. *Adv. Opt. Mater.* **2014**, *2*, 280−285.

(22) Park, S. J.; Hong, J. T.; Choi, S. J.; Kim, H. S.; Park, W. K.; Han, S. T.; Park, J. Y.; Lee, S.; Kim, D. S.; Ahn, Y. H. Detection of microorganisms using terahertz metamaterials. *Sci. Rep.* **2014**, *4*, 1−7.

(23) Ma, F.; Lin, Y.; Zhang, X.; Lee, C. Tunable multiband terahertz metamaterials using a reconfigurable electric split-ring resonator array. *Light: Sci. Appl.* **2014**, *3*, No. e171.

DOI: 10.1021/acsphotonics.5b00088
ACS Photonics 2015, 2, 890−898

(24) Ho, C. P.; Pitchappa, P.; Lin, Y.; Huang, C.; Kropelnicki, P.; Lee, C. Electrothermally actuated microelectromechanical systems based Omega-ring terahertz metamaterial with polarization dependent characteristics. *Appl. Phys. Lett.* **2014**, *104*, 1611040.
(25) Pitchappa, P.; Ho, C. P.; Lin, Y.; Kropelnicki, P.; Huang, C.; Singh, N.; Lee, C. Micro-electro-mechanically Tunable Metamaterial With Enhanced Electro-optic Performance. *Appl. Phys. Lett.* **2014**, *104*, 151104.
(26) Grosjean, T.; Mivelle, M.; Baida, F. I.; Burr, G. W.; Fischer, U. C. Diabolo Nanoantenna for Enhancing and Confining the Magnetic Optical Field. *Nano Lett.* **2011**, *11*, 1009−1013.
(27) Roxworthya, B. J.; Toussaint, K. C. Simultaneously tuning the electric and magnetic plasmonic response using capped bi-metallic nanoantennas. *Nanoscale* **2014**, *6*, 2270−2274.
(28) Yang, Y.; Dai, H. T.; Sun, X. W. Fractal diabolo antenna for enhancing and confining the optical magnetic field. *AIP Adv.* **2014**, *4*, 017123.
(29) Pitchappa, P.; Ho, C. P.; Kropelnicki, P.; Singh, N.; Kwong, D.; Lee, C. Micro-electro-mechanically switchable near infrared complementary metamaterial absorber. *Appl. Phys. Lett.* **2014**, *104*, 201114.
(30) Pitchappa, P.; Ho, C. P.; Kropelnicki, P.; Singh, N.; Kwong, D.; Lee, C. Dual band complementary metamaterial absorber in near infrared region. *J. Appl. Phys.* **2014**, *115*, 193109.
(31) Chen, K.; Adato, R.; Altug, H. Dual-band perfect absorber for multispectral plasmon-enhanced infrared spectroscopy. *ACS Nano* **2012**, *6*, 7998−8006.
(32) Albella, P.; Neubrech, F.; Huck, C.; Golmar, F.; Casanova, F.; Hueso, L. E.; Pucci, A.; Aizpurua, J.; Hillenbrand, R. Experimental Verification of the Spectral Shift between Near- and Far-Field Peak Intensities of Plasmonic Infrared Nanoantennas. *Phys. Rev. Lett.* **2013**, *110*, 203902.
(33) Zuloaga, J.; Nordlander, P. On the Energy Shift between Near-Field and Far-Field Peak Intensities in Localized Plasmon Systems. *Nano Lett.* **2011**, *11*, 1280−83.
(34) Nanfang, Y.; Patrice, G.; Mikhail, A. K.; Francesco, A.; Jean-Philippe, T. Light propagation with phase discontinuities: Generalized laws of reflection and refraction. *Science* **2012**, *334*, 333−337.
(35) Shafiei, F.; Monticone, F.; Le, K. Q.; Liu, X.; Hartsfield, T.; Li, X.; Alu, A. A subwavelength plasmonic metamolecule exhibiting magnetic-based optical Fano resonance. *Nat. Nanotechnol.* **2013**, *8*, 95−100.
(36) Maier, S. *Plasmonics: Fundamentals and Applications*; Springer: New York, 2007.
(37) Linden, S.; Enkrich, C.; Wegener, M.; Zhou, J.; Koschny, T.; Soukoulis, C. M. Magnetic Response of Metamaterials at 100 Terahertz. *Science* **2004**, *306*, 1351.
(38) Zhou, J.; Koschny, T.; Soukoulis, C. M. Magnetic and electric excitations in split ring resonators. *Opt. Exp.* **2007**, *5*, 17881−17890.
(39) Grefe, S. E.; Leiva, D.; Maste, S.; Dhuey, S. D.; Cabrini, S.; Schuckc, P. J.; Abate, Y. Near-field spatial mapping of strongly interacting multiple plasmonic infrared antennas. *Phys. Chem.* **2013**, *15*, 18944−18950.
(40) Lahiri, B.; Khokhar, A. Z.; De La Rue, R. M.; McMeekin, S. G.; Johnson, N. P. Asymmetric split ring resonators for optical sensing of organic materials. *Opt. Exp.* **2009**, *17*, 1107−1115.
(41) Clark, A. W.; Thompson, D. G.; Graham, D.; Cooper, J. M. Engineering DNA Binding Sites to Assemble and Tune Plasmonic Nanostructures. *Adv. Mater.* **2014**, *26*, 4286−4292.
(42) Shalaev, V. M. Optical negative-index metamaterials. *Nat. Photonics* **2007**, *1*, 41−48.
(43) Magnusson, R.; Wawro, D.; Zimmerman, S.; Ding, Y. Resonant Photonic Biosensors with Polarization-Based Multiparametric Discrimination in Each Channel. *Sensors* **2011**, *11*, 1476−1488.
(44) Zhang, N.; Liu, Y. J.; Yang, J.; Su, X.; Deng, J.; Chum, C. C.; Hong, M.; Teng, J. High sensitivity molecule detection by plasmonic nanoantennas with selective binding at electromagnetic hotspot. *Nanoscale* **2014**, *6*, 1416.
(45) Park, D. J.; Zhang, C.; Ku, J. C.; Zhou, Y.; Schatz, G. C.; Mirkin, C. A. Plasmonic photonic crystals realized through DNA-programmable assembly. *Proc. Natl. Acad. Sci. U.S.A.* **2015**, *112*, 977−981.
(46) Jiang, Q.; Wang, Z.-G.; Ding, B. Programmed Colorimetric Logic Devices Based on DNA−Gold Nanoparticle Interactions. *Small* **2013**, *9*, 1016−1020.

DOI: 10.1021/acsphotonics.5b00088
ACS Photonics 2015, 2, 890−898